Journal of Power Sources 262 (2014) 129–135

Contents lists available at ScienceDirect

Journal of Power Sources

journal homepage: www.elsevier.com/locate/jpowsour

Temperature dependent ageing mechanisms in Lithium-ion batteries – A Post-Mortem study

Thomas Waldmann*, Marcel Wilka, Michael Kasper, Meike Fleischhammer, Margret Wohlfahrt-Mehrens

ZSW – Zentrum für Sonnenenergie- und Wasserstoff-Forschung, Baden-Württemberg, Helmholtzstrasse 8, D-89081 Ulm, Germany

HIGHLIGHTS

- The ageing behaviour of cycled cells is tested in the range of −20 °C to +70 °C.
- Temperature dependent ageing mechanisms are found by an Arrhenius plot.
- The different ageing mechanisms are proven by Post-Mortem analysis.
- The reason for the different mechanisms is found by tests with reference electrodes.

GRAPHICAL ABSTRACT

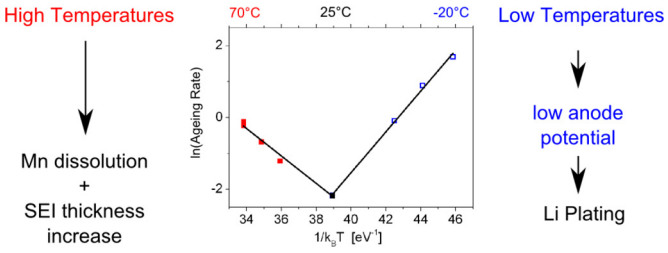

ARTICLE INFO

Article history:
Received 18 November 2013
Received in revised form
7 March 2014
Accepted 24 March 2014
Available online 31 March 2014

Keywords:
High-power Lithium-ion batteries
Ageing mechanisms
Electrode polarization
Arrhenius
Post-Mortem analysis
Battery life-time

ABSTRACT

The effects of temperatures in the range of −20 °C to 70 °C on the ageing behaviour of cycled Lithium-ion batteries are investigated quantitatively by electrochemical methods and Post-Mortem analysis. Commercial 18650-type high-power cells with a $Li_xNi_{1/3}Mn_{1/3}Co_{1/3}O_2/Li_yMn_2O_4$ blend cathode and graphite/carbon anode were used as test system. The cells were cycled at a rate of 1 C until the discharge capacity falls below 80% of the initial capacity. Interestingly, an Arrhenius plot indicates two different ageing mechanisms for the ranges of −20 °C to 25 °C and 25 °C to 70 °C. Below 25 °C, the ageing rates increase with decreasing temperature, while above 25 °C ageing is accelerated with increasing temperature. The aged 18650 cells are inspected via scanning electron microscopy (SEM), energy dispersive X-ray analysis (EDX), inductively coupled plasma (ICP), measurements of electrode thickness and X-ray diffraction (XRD) after disassembly to learn more about the chemical reasons of the degradation. The effect of different temperatures on the electrode polarizations are evaluated by assembling electrodes in pouch cells with reference electrode as a model system. We find that the dominating ageing mechanism for $T < 25$ °C is Lithium plating, while for $T > 25$ °C the cathodes show degeneration and the anodes will be increasingly covered by SEI layers.

1. Introduction

Besides the use of Lithium-ion batteries in portable devices, they are regarded as the key technology for the next generation of vehicles [1–3] and nearly all car manufacturers have already introduced one or more vehicles that utilize electric drive systems. Apart from major advantages of this technology, such as local zero emission vehicles and independence from the oil market, there are still problems regarding the life-time of car batteries. In order to improve the long-term usability of Lithium-ion batteries, it is essential to gather more knowledge about the chemical processes that contribute to battery ageing. The state-of-health (SOH) which

* Corresponding author. Tel.: +49 (0)731 9530 212; fax: +49 (0)731 9530 666.
E-mail address: thomas.waldmann@zsw-bw.de (T. Waldmann).

http://dx.doi.org/10.1016/j.jpowsour.2014.03.112
0378-7753/

determines the 'age' of a battery is commonly defined as the discharge capacity of an aged cell compared to the discharge capacity of the same cell when it was new. An SOH <80% is commonly regarded as end-of-life (EOL) criterion for a battery. The course of SOH as function of time during the ageing process is influenced by the conditions of operation of the battery and contains information on the ageing rate of the cell if the experimental conditions are well-defined. Such defined model conditions can for example be achieved by cycling at defined temperatures [4]. In order to learn more about ageing processes on the microscopic scale, there have been several studies regarding the ageing of electrodes [5,6], electrolyte [7–9] and separator materials [10] as well as the electrode | electrolyte interface [11–15]. Known ageing effects comprise Mn dissolution from the cathode [16–19] and subsequent deposition on the anode [5], Mn re-deposition on the cathode [20], particle cracks [21], loss of cyclable Li [22–24], Lithium plating [25,25–28] or solid–electrolyte interface (SEI) growth [13–15,24,27]. It was also shown that variations of the material composition can lead to improved batteries, e.g. by using additives [29,30] or blending of cathode materials [31–33]. Since it may take several years to reach the EOL criterion of a battery under moderate operation conditions, accelerated ageing tests are used. In such tests the batteries are put under stress for example by elevated temperatures [4,34–37], however, there is a lack of data on the ageing induced by low temperatures. The speed of ageing can quantitatively be described by ageing rates, which are contained in the capacity fade curves. After measuring ageing rates as a function of temperature, it is common practice to linearize the data by plotting $\ln(r)$ vs. $1/T$, which is known as Arrhenius plot [38,39] according to the equation

$$r = A \exp\left(-\frac{E_a}{k_B T}\right) \quad (1)$$

with the ageing rate r, the pre-exponential factor A, the activation barrier E_a and the Boltzmann constant k_B. Arrhenius theory has been used in the field of Lithium-ion batteries to determine activation barriers for ageing [36,40] and other processes [41–44]. However, it is often disregarded that the linear Arrhenius-like behaviour is only valid in certain temperature intervals. A change of the slope in an Arrhenius plot is an indication for a mechanism change [38]. Arrhenius behaviour has been observed for Lithium-ion batteries [14,36,45], but not over the whole temperature range which a battery electric car might be exposed to (−20 to 70 °C). In literature, ageing measurements are carried out mostly below 60 °C, since changes in the reaction mechanism are expected [4]. Only few authors performed tests at 65 °C [4], 70 °C [46] or 85 °C [47]. It depends on the battery chemistry and design at which temperature a change of the ageing mechanism occurs. Results on 18650 cells with $Li_xNi_{1/3}Mn_{1/3}Co_{1/3}O_2/Li_yMn_2O_4$ blend cathodes have been published before, however, different ageing conditions and electrochemical instead of Post-Mortem analysis was applied [24,27,48].

In this paper, we use temperatures in the range of −20 °C to 70 °C to accelerate the ageing of 18650 cells with blend cathodes under cycling conditions. By utilizing an Arrhenius plot, we find two different ageing mechanisms depending on the ageing temperature. The chemical reasons for the degradation mechanisms are identified by Post-Mortem analysis of the 18650 cells and by polarization measurements with pouch cells with reference electrode.

2. Experimental

The investigated commercial batteries used in this work have an initial capacity of 1.5 Ah and contain $Li_xNi_{1/3}Mn_{1/3}Co_{1/3}O_2/Li_yMn_2O_4$ blend cathodes and graphite/carbon anodes. All tested cells in the present study were very similar in mass, open circuit voltage, internal resistance and capacity at SOH = 100%, qualifying them for systematic ageing tests [48]. To compensate the small variations in the capacities and internal resistances of the new batteries, both values are relating to those of the respective un-aged batteries and are specified in %. The cells were aged inside climate chambers (Vötsch) and electrochemical measurements were conducted using a Basytec CTS system. All charging procedures during cycling and capacity tests were done using a constant current/constant voltage (CCCV) test protocol, while the discharge was conducted with constant current (CC). The cycled cells were charged and discharged between 2.0 V and 4.2 V with 1.5 A (1 C) in all cases. The stop criterion for all ageing tests was SOH = 80% with respect to discharging at a rate of 1 C at 25 °C. At different points in time during the ageing tests, the tests were interrupted for capacity tests (see Fig. 2). For comparability reasons, the cells were allowed to relax to 25 °C and capacities were measured at a rate of 1 C. Subsequently, the ageing tests were continued, if the EOL criterion was not fulfilled. Ageing rates were determined tangential from the slope SOH(t) vs. t plots with the intercept point SOH($t = 0$) = 100%. Before the disassembly by a high precision saw, the 18650 cells were discharged to their end-of-discharge voltage of 2.0 V, to keep both, risk and corrosion issues low. The electrodes were separated and washed with DMC by using a self developed washing procedure until the remaining conductive salt concentration was reduced to a no more analytically significant value. The electrode samples taken from the outer part of the jelly rolls were analyzed by SEM/EDX (LEO 1530VP Gemini), ICP and XRD. The X-ray diffraction was performed with a Siemens D5000 (CuKα radiation in reflection geometry). The lattice parameters were refined by means of the whole-powder pattern decomposition (WPPD) method (Pawley) using TOPAS (Bruker). Polarization values were calculated with respect to the second cycle at 25 °C and 1 C.

3. Results and discussion

3.1. Un-aged commercial 18650 cells

First, the un-aged 18650 batteries were characterized, in order to compare the results with those from the aged cells. ICP measurements showed a 1:1 ratio for the $Li_xNi_{1/3}Mn_{1/3}Co_{1/3}O_2$:$Li_yMn_2O_4$ blend. The chemical composition of single particles $Li_xNi_{1/3}Mn_{1/3}Co_{1/3}O_2$ was determined by EDX point spectra to be 1:1:1 under consideration of the excitation radius and within the error bars. The anode consists of spherical graphite and carbon particles (Fig. 1a). For the anode material, the blend ratio is not accessible with our methods. ICP did not show significant amounts of Mn on the new anodes. The X-ray diffraction patterns of the un-aged cathodes show reflections corresponding to the layer structure R-3m (hexagonal setting) and the spinel structure (Fd-3m). XRD of un-aged cathodes revealed the lattice constants a(NMC) = 2.857703(255) Å, c(NMC) = 14.24968(245) for $Li_xNi_{1/3}Mn_{1/3}Co_{1/3}O_2$ and $a(Li_yMn_2O_4)$ = 8.21033(95) Å for $Li_yMn_2O_4$.

3.2. Arrhenius behaviours of capacity fade in different temperature ranges

18650 cells were cycled with charge and discharge rates of 1 C at constant temperatures between −20 °C and 70 °C. As can be seen in Fig. 2, SOH(t) is a nearly linear function in the SOH range of 100%–90%, as indicated by R^2-values larger than 0.97, except for $T = 25$ °C where $R^2 = 0.93$. For cycling at 1 C at 25 °C, the curve shape of the SOH(t) data in Fig. 2 is similar to the data reported by Dubarry et al., who cycled NMC/LMO blend cells at a rate of 2 C [24]. Comparing

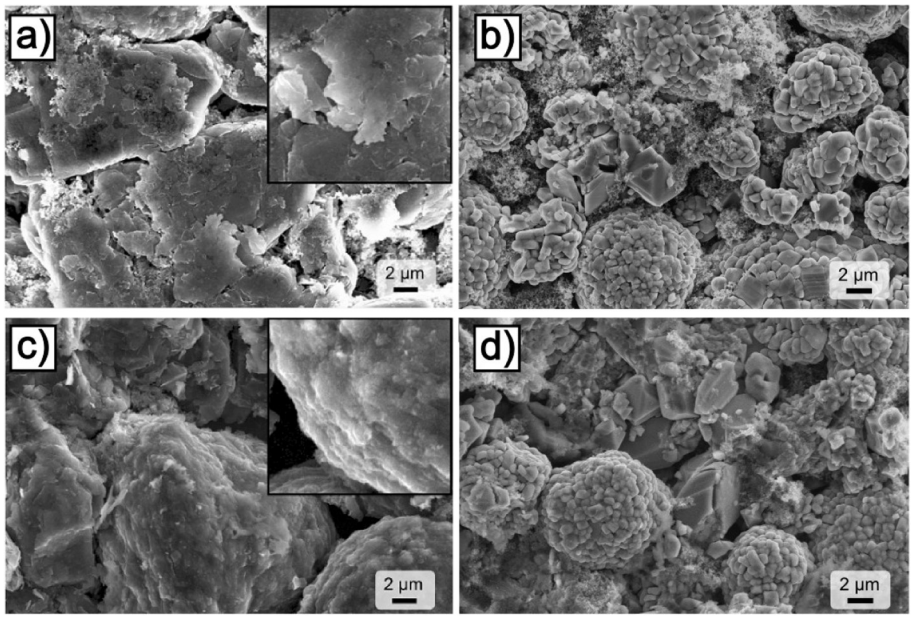

Fig. 1. SEM images (magnification: 10^4) of an un-aged (SOH = 100%) a) anode and b) blend cathode and an aged (SOH = 80%, cycled at $T = 70$ °C) c) anode and d) blend cathode. Insets in a) and c) show magnifications of graphite particles. The aged anode shows increased SEI thickness (compare (a) and (c)), while the aged cathode looks similar to its un-aged situation (compare (b) and (d)).

the number of cycles until 80% SOH is reached at 25 °C is similar in our study (638 cycles) compared to the cells cycled at 2 C by Dubarry et al. (~610 cycles) [24] if the capacity loss measured at 1 C are compared.

The fitting of the SOH(t) data allows us to obtain ageing rates r as a function of temperature. In the temperature range between 25 °C and 70 °C (high temperature range, red data points in all graphs), we find the clear trend of rising ageing rates with increasing temperature. This is in accordance with other studies on the ageing of Lithium-ion batteries [4,34–37] and the general principle that chemical reactions are accelerated with increasing temperature [38,39]. This indicates that the change of the SOH of the batteries cycled in the high temperature range is directly related to chemical degradation reactions (see also Post-Mortem analysis below).

On the other hand, between 25 °C and −20 °C (low temperature range, blue data points in all graphs), this trend is reversed, leading to higher ageing rates with decreasing temperature. For example, it can be seen from Fig. 2 that SOH(t) decreases approximately with the same rate for $T = 70$ °C and for $T = 0$ °C. Such a trend was also reported in literature, but for $T = 50$ °C and $T = 25$ °C [23]. The ageing behaviour in the low temperature range is obviously not consistent with a chemical reaction that is directly responsible for the battery degradation.

The difference between the two temperature ranges is clearly visible in the Arrhenius plot in Fig. 3, where two straight lines with different slopes can be drawn for the two temperature ranges. Since a change in the slope in an Arrhenius plot is associated with a mechanism change [38], we can already conclude at this point that there are two different ageing mechanisms for temperatures below and above 25 °C. In particular, the slope for the high temperature range is negative and it corresponds to an activation barrier of $E_{a,HT} = 0.38 \pm 0.02$ eV ($R^2 = 0.99$) for the ageing reaction. This is consistent with the range of values for activation barriers obtained by Liaw et al. which are in a range of 0.33–0.57 eV [36]. For the Arrhenius-plot it is important to use rates with the unit 1/time.

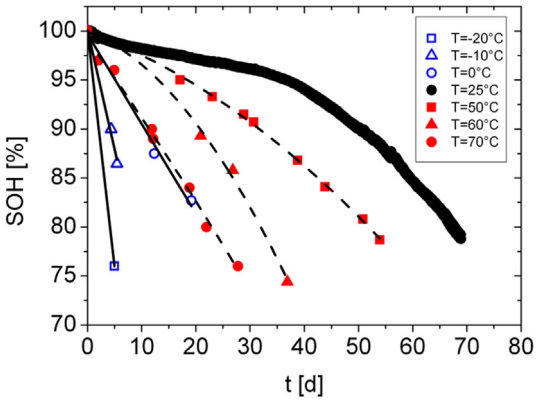

Fig. 2. Measured SOH curves as a function of time for cycling at a rate of 1 C and different temperatures. In the case of $T = 25$ °C all data is shown, for all other tests, only capacity measurements at 25 °C are plotted. The solid and dashed lines are drawn to guide the eye for the tests below and above $T = 25$ °C, respectively.

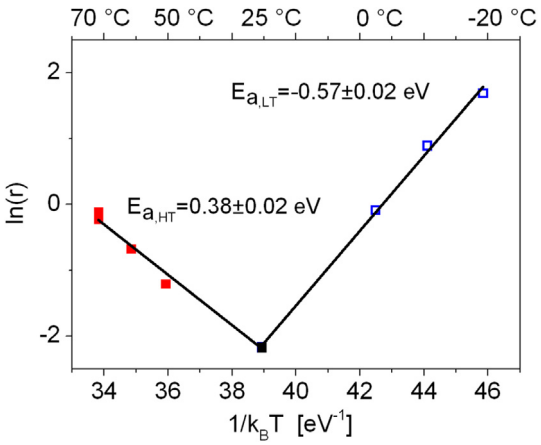

Fig. 3. Arrhenius plot for the ageing behaviour of 18650 cells cycled at 1 C in a temperature range of −20 °C to 70 °C. The solid lines correspond to linear fits of the data points of the respective temperature ranges below and above 25 °C.

Zhang et al. obtained significantly lower values for their activation energies, because they did not use rates, but discharge capacities in their plot [40]. Thus, their barriers are not directly comparable to our data. Similar values for barriers were also reported for the energy barriers for diffusion of Li ions in Li_xC_6 [49] or in $Li_xMn_2O_4$ [50] or for bond strengths of ionic bonds (0.1–1.0 eV) [51]. The barrier for intercalation of Li ions passing the SEI and intercalating into graphite is also in a similar range (0.4–0.6 eV) [42,44].

For the low temperature range ($T < 25$ °C), the slope fitted to the respective points in the Arrhenius plot is positive, resulting in an apparent negative activation barrier of $E_{a,LT} = -0.57 \pm 0.02$ eV ($R^2 = 0.99$). Negative barriers are known from physical chemistry textbooks [38,39], but were to best of our knowledge not reported for ageing of Lithium-ion batteries. The apparent negative activation barrier indicates a fast exothermic equilibrium located before the actual ageing reaction changing the sign in the exponent of the Arrhenius equation (see Equation (1)) [38]. In our experiments, this equilibrium could be related to exothermic adsorption/desorption processes of electrolyte molecules on the Li surface (plated on the anode), previous to reaction of adsorbed electrolyte with metallic Li. It is obvious that reactions at freshly formed Li metal | electrolyte interfaces are likely to occur during deposition and dissolution of Li metal. Such reactions lead to consumption of cyclable Li and thus contribute to capacity loss [22,26].

In the 18650 cells, we were not able to observe Lithium plating after cycling in the low temperature range directly because the 18650 cells could only be opened in the discharged state, where the plated Li might have been dissolved. Furthermore, the pressure in round cells is higher compared to pouch cells, which may lead to a higher reversibility of the plating. Nevertheless, we found a widespread white deposition on the anodes of aged 18650 cells cycled in the low temperature range, which was absent in the high temperature range. However, the occurrence of Lithium plating in the low temperature range is supported by the following measurements.

1) We find a very similar ageing rate r for the following two experiments: For 18650 cells cycled (charged and discharged) at −20 °C ($r = 5.4\%$/d) and for cells which are charged at −20 °C but discharged at 25 °C ($r = 7.6\%$/d). In contrast, cells charged at 25 °C and discharged at −20 °C have an ageing rate that is ∼10 times slower compared to the above cases ($r = 0.57\%$/d). This shows that the accelerated ageing at low temperature is related to the charging procedure, in which the Li plating occurs.
2) We find a significantly lower coulomb efficiency for cells cycled at low temperature. This was also observed by Downie et al. during Lithium plating [26]. In particular, we measured a mean coulomb efficiency for the first seven cycles of 0.975 for −20 °C and 0.999 for 25 °C. These values are consistent with the trend reported by Downie et al. for charging with and without plating, respectively [26].
3) The anodes of model pouch cells with reference electrodes (see below) were plated with grey coloured metallic Li after cycling in the low temperature range, but not in the high temperature range (see insets in Fig. 8).

In order to get more detailed insights on the chemical processes leading to the observed capacity fade, we performed Post-Mortem analysis with the 18650 cells, aged until an SOH of 80% was reached. These results are presented in the following two sections.

3.3. Increasing SEI thickness as cause of resistance increase

From SEM images of the anodes of aged cells, we find that anode particles are covered by a thick SEI film (Fig. 1c). As can be seen from Fig. 1a, the SEI is less pronounced on the anode particles of un-aged cells, however, a quantitative evaluation of the SEI thickness is not possible from the SEM images and it is difficult to see differences between cells cycled at low and high temperatures.

Thus, we performed thickness measurements with electrodes from 18650 cells cycled at different temperatures. Since all electrodes were subject to the same preparation procedure they can be compared among each other. For the anodes aged at $T \geq 25$ °C, we find an increase of thickness compared to un-aged anodes, which we attribute to the SEI film growth on the anode particles (Fig. 4b). As expressed in Fig. 5a, b, the thickness of the SEI on the single anode particles adds up to a macroscopic value, that is measurable in the overall anode thickness. In contrast, the electrode thickness for $T \leq 0$ °C is nearly constant (∼86 μm) and corresponds to that of un-aged anodes ($d \approx 85$ μm). This shows already that there is a difference in the growth of SEI thickness in the low and high temperature ranges.

For the cathode particles, we do not see the formation of a film in the SEM images when comparing cathodes of aged and un-aged cells (Fig. 1b, d). This is consistent with the fact that the cathode thickness is independent to the ageing temperature and similar for un-aged and aged electrodes ($d \approx 96$ μm). Thus, the impedance rise of the cells cannot be explained by a thickness increase of the SEI layer on the cathode.

In contrast, we find that the thickness d of the anode correlates well with the internal resistance of the cells (Fig. 5c). This leads us to the conclusion that in our ageing experiments, the SEI growth of the anodes contributes to the resistance of the battery in contrast to SEI growth on the cathodes. Since this correlation exists over the whole temperature (see Fig. 5c) range of −20 °C to 70 °C, this can be regarded as a general trend. The chemical composition of the SEI films on the aged electrodes was further investigated by ICP and EDX measurements. Typical elements that can be expected for SEI layers are Li, P, F, O, S and organic compounds [15,52]. Mn is known to dissolve from cathodes and

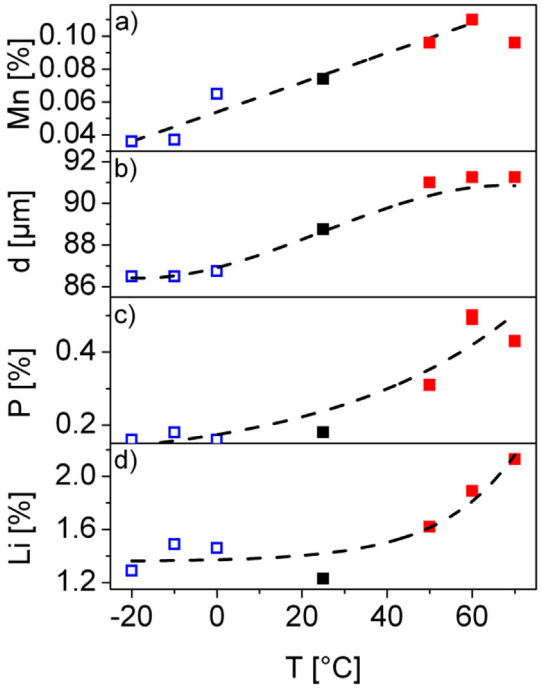

Fig. 4. Results of the Post-Mortem analysis of anodes from 18650 cells cycled at different temperatures. a) Mn content, b) anode thickness, c) P content and d) Li content. The dashed lines are drawn to guide the eye.

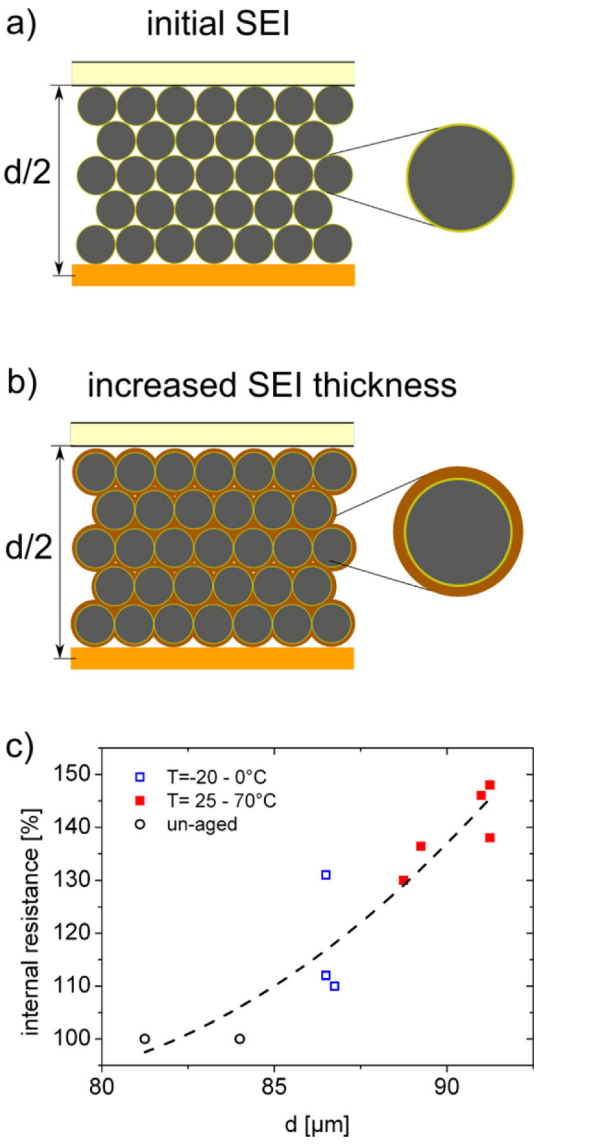

Fig. 5. Model for the explanation of anode thickness *d*. The grey objects represent the carbon/graphite spheres of the anode, the SEI formed during formation of the battery is coloured green and the SEI films growing during ageing are illustrated in brown colour. The anode thickness in (b) is increased in comparison to (a). c) Correlation of anode thickness *d* and internal resistance of 18650 cells. The dashed line is drawn to guide the eye. (For interpretation of the references to colour in this figure legend, the reader is referred to the web version of this article.)

after transport through the electrolyte to be found on the anodes [16–18] of aged cells.

In the text below, we discuss the ICP results limited to the elements Li, P and Mn. Our EDX results show the same trends as ICP for all analyzed elements and are thus not shown in detail here.

As can be seen from Fig. 4c, d, the Li and P content of the anode is similar for $T \leq 25$ °C and increases with temperature for $T > 25$ °C. Furthermore, the P content of both electrodes is similar for the aged and un-aged cases for $T \leq 25$ °C. This is consistent with the trend of the increase of SEI thickness in Fig. 4b and with literature [14]. In case of the cathodes, the P content found by ICP is significantly lower than for the anodes, in accordance with an SEI growth happening preferentially on the anodes as shown above by the thickness measurements.

Due to these findings, we attribute the origin of SEI growth in our battery system to the decomposition of electrolyte at the anode|electrolyte interface. In particular, we find P and Li originating from decomposed conductive salt. This leads to a decrease in cyclable Li ions which are consumed to form additional SEI.

A similar degradation mechanism was suggested before from electrochemical characterization of 18650-type cells with NMC/LMO blend cathode for temperatures around 50–60 °C [27].

The additional Li found on aged anodes in the present study is correlated to a Li loss from the cathode with respect to the Li content of un-aged cells. As shown in Fig. 6a, this is a general trend over the whole temperature range.

Loss of active material was suggested from electrochemical tests involving 18650 cells with NMC/LMO blend cathodes [24,27] and was detected indirectly in the present study for Mn dissolved from the cathode by Post-Mortem analysis. As shown in Fig. 4a, The Mn content of the anode increases nearly linearly with temperature from $T = -20$ °C to 60 °C. On the cathode, we are not able to detect the Mn loss by our ICP or EDX methods. The Mn traces found on the anodes by ICP and EDX, especially at elevated temperatures, indicate also a degradation of cathode, which could also be related to resistance increase of the cells [19].

3.4. Structural degradation of the cathode during thermal ageing

The XRD of the thermally aged cathode shows structural changes depending on the temperature. In case of $Li_xNi_{1/3}Mn_{1/3}Co_{1/3}O_2$, a significant lattice expansion along the *c*(NMC)-axis and a small contraction along the *a*(NMC)-axis take place with increasing temperature (Fig. 7a, b). Simultaneously, the lattice constant *a*($Li_yMn_2O_4$) decreases with increasing temperature (Fig. 7c). Hence, the change of the NMC lattice constants correlates very well with the Li-loss at the cathode (see Fig. 6b, c). We cannot explain the different behaviour of the data point at 0 °C and believe it is an outlier. The removal of Li from the $Li_xNi_{1/3}Mn_{1/3}Co_{1/3}O_2$ structure is connected with the oxidation of $Ni^{2+} \rightarrow Ni^{3+} \rightarrow Ni^{4+}$ and therefore with a decrease of the Ni ionic radii. This leads to the decrease of the lattice constant *a*(NMC). However, we note, that Ni was not found on the anodes. The increase of *c*(NMC) is due to the electrostatic repulsion of oxygen–oxygen growing with the Li extraction [53,54]. The correlation between the Li-loss of the cathode and the change of the $Li_yMn_2O_4$ lattice constants is not as clear as in the case of $Li_xNi_{1/3}Mn_{1/3}Co_{1/3}O_2$. In general, the lattice parameter *a*(LMO) of $Li_yMn_2O_4$ decreases during Li removal due to the coupled increase of smaller Mn^{4+} [55,56]. The Mn deposition at the anode, determined by ICP analysis, is very likely caused by Mn^{2+} dissolution from the $Li_yMn_2O_4$ structure. This process is well known [16,57,58] and based on the disproportion of $Mn^{3+} \rightarrow Mn^{4+} + Mn^{2+}$ (solv).

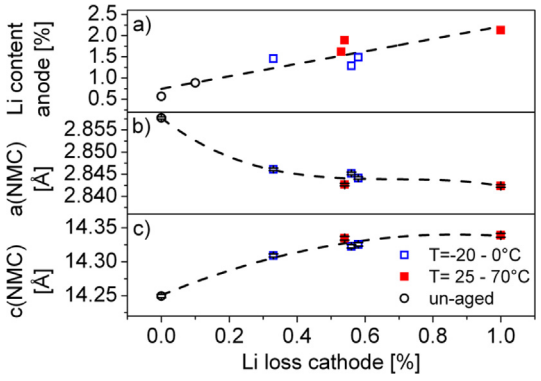

Fig. 6. Li loss in cathodes correlated to a) Li content in anodes as measured by ICP. b) Lattice constant *a*(NMC) and c) *c*(NMC) of $Li_xNi_{1/3}Mn_{1/3}Co_{1/3}O_2$ as measured by XRD. The dashed lines are drawn to guide the eye.

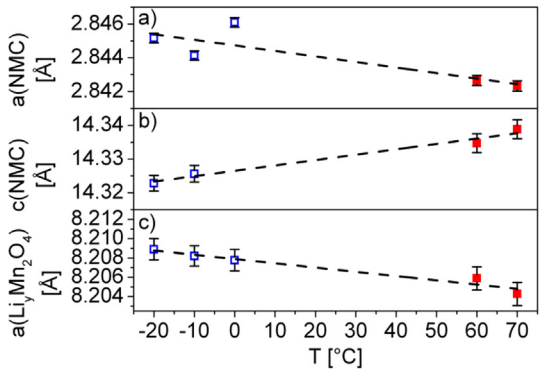

Fig. 7. Results of cathode analysis for 18650 cells cycled at different temperatures. Lattice constants from XRD measurements are shown a) a(NMC), b) c(NMC) and c) $a(Li_yMn_2O_4)$. The dashed lines are drawn to guide the eye.

The lattice parameter $a(Li_yMn_2O_4)$ decreases due to the formation of the smaller Mn^{4+} ions. The observed decrease of $a(Li_yMn_2O_4)$ during thermal ageing can therefore be explained by Li and/or Mn extraction from the $Li_yMn_2O_4$ spinel structure.

We conclude that the Mn loss on the cathode is related to degradation of both, cathode and anode. In contrast, the Li loss of the cathode is not an ageing effect of the cathode. As the 'lost' Li that cannot be found in the cathode after discharging of the cells is detected mostly in the SEI of the anode, the Li loss indicates a degradation of the anode but not a deterioration of the cathode. This shows that interactions of anode and cathode play an important role in the ageing of Lithium-ion batteries and suggests the use of full cells rather than half cells for ageing tests.

3.5. Anode polarization as cause of ageing at low temperatures

The origin of the Lithium plating at low temperatures during cycling at 1 C was further investigated by pouch cells with Li reference electrodes. Two types of pouch cells were prepared with $Li_xNi_{1/3}Mn_{1/3}Co_{1/3}O_2$ as the common cathode material and either amorphous carbon or graphite as anode material.

Fig. 8a shows the electrode polarization vs. Li/Li^+ in the temperature range between 20 °C and −10 °C. There is the clear trend that both, amorphous carbon and graphite anodes are more polarized at lower temperatures. This is consistent with results of Lin et al., who reported about a lower anode potential during charging at −20 °C compared to charging at room temperature [25].

For the graphite anode, this effect is stronger pronounced than for amorphous carbon. This can be explained by differences in the charge transfer resistances through the SEI, since the diffusion through the SEI is temperature dependent [59,60]. The fact that the graphite anode is below 0 V in this temperature range leads to plating of the anodes with metallic Li [25]. As experimental proof for the relationship between the negative anode polarization with respect to Li/Li^+, we opened the pouch cells and found that the anodes were indeed plated with grey metallic Li (see inset of Fig. 8a). This finding is in agreement with literature [25,27,28].

Fig. 8b shows the anode polarization for a temperature range between 35 °C and 60 °C. Again, the data show a more positive polarization with respect to Li/Li^+ with increasing temperature. In contrast to the low temperature range, we find a smaller difference between the polarization behaviour of amorphous carbon and graphite anodes. In the high temperature range, the polarization is positive with respect to Li/Li^+, which does not lead to Lithium plating on the anodes, as proven by opening of the pouch cells (see inset of Fig. 8b).

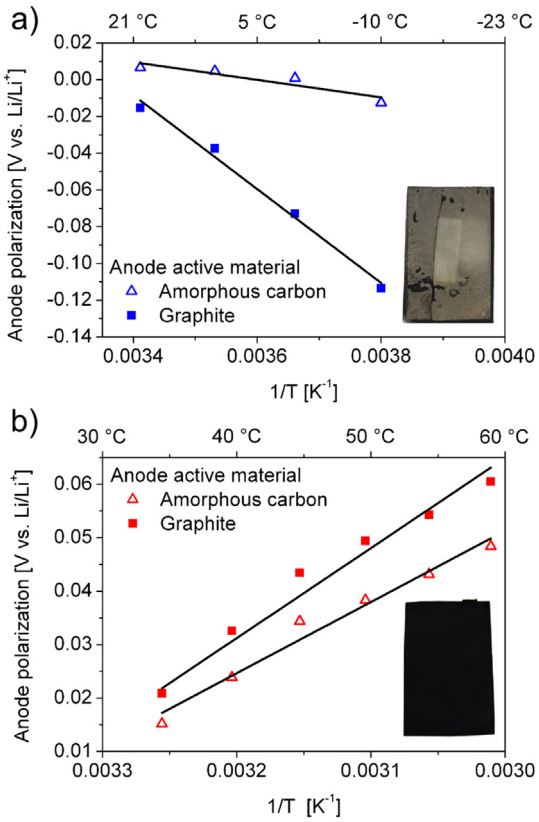

Fig. 8. Anode polarization vs. Li/Li^+ measured in pouch cells with amorphous carbon/graphite anodes, NMC cathodes and reference electrode. a) Low temperature range, b) high temperature range. The insets show photographs of the anodes from pouch cells which are typical for the respective temperature range.

4. Conclusions

We tested commercial 18650 cells with $Li_xNi_{1/3}Mn_{1/3}Co_{1/3}O_2$/$Li_yMn_2O_4$ blend cathodes and graphite/carbon anodes. The cells were cycled in a temperature range between −20 °C and 70 °C until an SOH limit of ~80% was reached. An Arrhenius plot reveals two different ageing mechanisms below and above 25 °C. Below 25 °C, we find that the predominant ageing mechanism is plating of metallic Lithium on the anodes and subsequent reaction with the electrolyte, leading to loss of cyclable Lithium. The occurrence of Lithium plating is explained by measurements with Pouch cells with reference electrode that show a negative polarization with respect to Li/Li^+ in the low temperature range. Above 25 °C, the polarization vs. Li/Li^+ of the anodes is positive, preventing Lithium plating. Instead, the elevated temperatures accelerate other degradation reactions, namely degradation of the cathode and SEI film growth on the anode, leading to capacity fade and internal resistance increase. Our tests show also interactions between anode and cathode which can only be observed in full cells. In particular, we find Mn deposition on anodes which is related to degradation of the cathode and a thicker SEI on the anode containing Li which cannot be intercalated into the cathode. The tested cells exhibit the slowest ageing for $T = 25$ °C, showing the importance of cooling and heating systems in battery packs for automotive applications, which may be used in a short-term time scale. However, on a medium-term time scale, batteries have to be improved to be resistant against ageing in a wide temperature range, e.g. by development of new materials or material combinations. In particular, Lithium plating has to be prevented at low temperatures and reactions at the electrode | electrolyte interface

and dissolution from cathodes have to be prevented at high temperatures.

Acknowledgement

The authors would like to thank D. Rosato and N. Dorsch from Robert Bosch GmbH for providing the cells within the common research project (ReLiOn, contract no. 03X4619C), funded by the German Federal Ministry of Education and Research (BMBF) and managed by the Project Management Agency Forschungszentrum Jülich (PTJ). We thank Gerda Dörfner for SEM/EDX and Barbara Zwikirsch/Gisela Arnold for ICP measurements. The responsibility for this publication rests with the authors.

References

[1] J.B. Goodenough, Y. Kim, Chem. Mater. 22 (2010) 587.
[2] M. Armand, J.-M. Tarascon, Nature 451 (2008) 652.
[3] B. Scrosati, J. Garche, J. Power Sources 195 (2010) 2419.
[4] M. Ecker, J.B. Gerschler, J. Vogel, S. Käbitz, F. Hust, P. Dechent, D.U. Sauer, J. Power Sources 215 (2012) 248.
[5] A. Blyr, C. Sigala, G. Amatucci, D. Guyomard, Y. Chabre, J.M. Tarascon, J. Electrochem. Soc. 145 (1998) 194.
[6] V. Agubra, J. Fergus, Materials 6 (2013) 1310.
[7] G. Gachot, P. Ribière, D. Mathiron, S. Grugeon, M. Armand, J.-B. Leriche, S. Pilard, S. Laruelle, Anal. Chem. 83 (2011) 478.
[8] G. Gachot, S. Grugeon, M. Armand, S. Pilard, P. Guenot, J.-M. Tarascon, S. Laruelle, J. Power Sources 178 (2008) 409.
[9] L. Gireaud, S. Grugeon, S. Pilard, P. Guenot, J.-M. Tarascon, S. Laruelle, Anal. Chem. 78 (2006) 3688.
[10] C. Peabody, C.B. Arnold, J. Power Sources 196 (2011) 8147.
[11] D. Aurbach, E. Zinigrad, Y. Cohen, H. Teller, Solid State Ionics 148 (2002) 405.
[12] W. Li, B.L. Lucht, J. Electrochem. Soc. 153 (2006) A1617.
[13] E. Peled, J. Electrochem. Soc. 126 (1979) 2047.
[14] M. Broussely, S. Herreyre, P. Biensan, P. Kasztejna, K. Nechev, R. Staniewicz, J. Power Sources 97–98 (2001) 13.
[15] E. Peled, D. Golodnitsky, C. Menachem, D. Bar-Tow, J. Electrochem. Soc. 145 (1998) 3482.
[16] J.M. Tarascon, W.R. McKinnon, F. Coowar, T.N. Bowmer, G. Amatucci, D. Guyomard, J. Electrochem. Soc. 141 (1994) 1421.
[17] M. Wohlfahrt-Mehrens, C. Vogler, J. Garche, J. Power Sources 127 (2004) 58.
[18] J. Vetter, P. Novák, M.R. Wagner, C. Veit, K.-C. Möller, J.O. Besenhard, M. Winter, M. Wohlfahrt-Mehrens, C. Vogler, A. Hammouche, J. Power Sources 147 (2005) 269.
[19] J. Park, J.H. Seo, G. Plett, W. Lu, A.M. Sastry, Electrochem. Solid-State Lett. 14 (2011) A14.
[20] D. Kim, S. Park, O.B. Chae, J.H. Ryu, Y.-U. Kim, R.-Z. Yin, S.M. Oh, J. Electrochem. Soc. 159 (2012) A193.
[21] K. Zhao, M. Pharr, J.J. Vlassak, Z. Suo, J. Appl. Phys. 108 (2010) 073517.
[22] J. Christensen, J. Newman, J. Electrochem. Soc. 152 (2005) A818.
[23] O. Dolotko, A. Senyshyn, M.J. Muhlbauer, K. Nikolowski, F. Scheiba, H. Ehrenberg, J. Electrochem. Soc. 159 (2012) A2082.
[24] M. Dubarry, C. Truchot, B.Y. Liaw, K. Gering, S. Sazhin, D. Jamison, C. Michelbacher, J. Power Sources 196 (2011) 10336.
[25] H.-P. Lin, D. Chua, M. Salomon, H.-C. Shiao, M. Hendrickson, E. Plichta, S. Slane, Electrochem. Solid-State Lett. 4 (2001) A71.
[26] L.E. Downie, L.J. Krause, J.C. Burns, L.D. Jensen, V.L. Chevrier, J.R. Dahn, J. Electrochem. Soc. 160 (2013) A588.
[27] M. Dubarry, C. Truchot, B.Y. Liaw, K. Gering, S. Sazhin, D. Jamison, C. Michelbacher, J. Electrochem. Soc. 160 (2013) A191.
[28] G. Park, N. Gunawardhana, H. Nakamura, Y.-S. Lee, M. Yoshio, J. Power Sources 199 (2012) 293.
[29] K. Amine, Z. Chen, Z. Zhang, J. Liu, W. Lu, Y. Qin, J. Lu, L. Curtis, Y.-K. Sun, J. Mater. Chem. 21 (2011) 17754.
[30] J. Liu, Z. Chen, S. Busking, I. Belharouak, K. Amine, J. Power Sources 174 (2007) 852.
[31] T. Numata, C. Amemiya, T. Kumeuchi, M. Shirakata, M. Yonezawa, J. Power Sources 97–98 (2001) 358.
[32] Z.F. Ma, X.Q. Yang, X. Sun, J. McBreen, J. New Mater. Electrochem. Syst. (2001) 121.
[33] H. Kitao, T. Fujihara, K. Takeda, N. Nakanishi, T. Nohma, Electrochem. Solid-State Lett. 8 (2005) A87.
[34] I. Bloom, B. Cole, J. Sohn, S. Jones, E. Polzin, V. Battaglia, G. Henriksen, C. Motloch, R. Richardson, T. Unkelhaeuser, D. Ingersoll, H. Case, J. Power Sources 101 (2001) 238.
[35] R. Spotnitz, J. Power Sources 113 (2003) 72.
[36] B.Y. Liaw, E.P. Roth, R.G. Jungst, G. Nagasubramanian, H.L. Case, D.H. Doughty, J. Power Sources 119–121 (2003) 874.
[37] R. Deshpande, M. Verbrugge, Y.-T. Cheng, J. Wang, P. Liu, J. Electrochem. Soc. 159 (2012) A1730.
[38] P.W. Atkins, Physical Chemistry, Oxford University Press, Oxford; New York, 1990.
[39] F.G. Helfferich, Kinetics of Multistep Reactions, Elsevier, Amsterdam; Boston, 2004.
[40] Y. Zhang, C.-Y. Wang, J. Electrochem. Soc. 156 (2009) A527.
[41] T. Abe, H. Fukuda, Y. Iriyama, Z. Ogumi, J. Electrochem. Soc. 151 (2004) A1120.
[42] Z. Ogumi, T. Abe, T. Fukutsuka, S. Yamate, Y. Iriyama, J. Power Sources 127 (2004) 72.
[43] Y. Yamada, Y. Iriyama, T. Abe, Z. Ogumi, Langmuir 25 (2009) 12766.
[44] J.P. Schmidt, T. Chrobak, M. Ender, J. Illig, D. Klotz, E. Ivers-Tiffée, J. Power Sources 196 (2011) 5342.
[45] R. Bouchet, S. Lascaud, M. Rosso, J. Electrochem. Soc. 150 (2003) A1385.
[46] A.M. Andersson, D.P. Abraham, R. Haasch, S. MacLaren, J. Liu, K. Amine, J. Electrochem. Soc. 149 (2002) A1358.
[47] L. Bodenes, R. Dedryvere, H. Martinez, F. Fischer, C. Tessier, J.-P. Peres, J. Electrochem. Soc. 159 (2012) A1739.
[48] M. Dubarry, C. Truchot, M. Cugnet, B.Y. Liaw, K. Gering, S. Sazhin, D. Jamison, C. Michelbacher, J. Power Sources 196 (2011) 10328.
[49] K. Persson, V.A. Sethuraman, L.J. Hardwick, Y. Hinuma, Y.S. Meng, A. van der Ven, V. Srinivasan, R. Kostecki, G. Ceder, J. Phys. Chem. Lett. 1 (2010) 1176.
[50] C.Y. Ouyang, S.Q. Shi, Z.X. Wang, H. Li, X.J. Huang, L.Q. Chen, Europhys. Lett. 67 (2004) 28.
[51] K. Xu, J. Electrochem. Soc. 154 (2007) A162.
[52] E. Peled, D. Bar Tow, A. Merson, A. Gladkich, L. Burstein, D. Golodnitsky, J. Power Sources 97–98 (2001) 52.
[53] Y.W. Tsai, B.J. Hwang, G. Ceder, H.S. Sheu, D.G. Liu, J.F. Lee, Chem. Mater. 17 (2005) 3191.
[54] S.-T. Myung, S. Komaba, K. Kurihara, K. Hosoya, N. Kumagai, Y.-K. Sun, I. Nakai, M. Yonemura, T. Kamiyama, Chem. Mater. 18 (2006) 1658.
[55] T. Ohzuku, M. Kitagawa, T. Hirai, J. Electrochem. Soc. 137 (1990) 769.
[56] S. Mukerjee, T.R. Thurston, N.M. Jisrawi, X.Q. Yang, J. McBreen, M.L. Daroux, X.K. Xing, J. Electrochem. Soc. 145 (1998) 466.
[57] Y. Terada, Y. Nishiwaki, I. Nakai, F. Nishikawa, J. Power Sources 97–98 (2001) 420.
[58] A. Du Pasquier, A. Blyr, P. Courjal, D. Larcher, G. Amatucci, B. Gérand, J.M. Tarascon, J. Electrochem. Soc. 146 (1999) 428.
[59] J. Fan, S. Tan, J. Electrochem. Soc. 153 (2006) A1081.
[60] M.C. Smart, J.F. Whitacre, B.V. Ratnakumar, K. Amine, J. Power Sources 168 (2007) 501.